ACS Catalysis

Research Article

pubs.acs.org/acscatalysis

Using Thiol Adsorption on Supported Au Nanoparticle Catalysts To Evaluate Au Dispersion and the Number of Active Sites for Benzyl Alcohol Oxidation

Basu Panthi,[†] Ahana Mukhopadhyay,[‡] Luke Tibbitts,[†] Johnny Saavedra,[†] Christopher J. Pursell,[†] Robert M. Rioux,[‡,§] and Bert D. Chandler*[,†]

[†]Department of Chemistry, Trinity University, San Antonio, Texas 78212-7200, United States

[‡]Department of Chemical Engineering and [§]Department of Chemistry, The Pennsylvania State University, University Park, Pennsylvania 16802-4400, United States

Supporting Information

ABSTRACT: Two techniques to study the surface chemistry of supported gold nanoparticles were developed. First, phenylethyl mercaptan (PEM) adsorption from hexane solution was followed with UV−vis spectroscopy to evaluate the total amount of surface Au available. Two catalysts, Au/Al_2O_3 and Au/TiO_2, were found to have Au:S surface stoichiometries of ∼2:1, whereas a Au/SiO_2 catalyst had a Au:S surface stoichiometry of ∼1:1. The room temperature equilibrium binding constants for PEM adsorption on the Au/Al_2O_3 and Au/TiO_2 catalysts were similar (∼3 × 10^5 M^{-1}; $\Delta G \approx -31$ kJ/mol); the PEM−Au/SiO_2 binding constant was somewhat larger (∼2 × 10^6 M^{-1}; $\Delta G \approx -36$ kJ/mol). XPS data for all of the catalysts showed no observable changes in the Au oxidation state upon adsorption of the thiol. Implications of these experiments regarding self-assembled monolayers and thiol-stabilized Au nanoparticles are discussed. Second, kinetic titrations (i.e., controlled thiol-poisoning experiments) were developed as a method for evaluating the number of active sites for selective 4-methoxybenzyl alcohol oxidation. These experiments suggested only a fraction of the surface Au (∼10−15% of the total Au) was active for the reaction. When thiol was added with the 4-methoxybenzyl alcohol substrate, more thiol was required to poison the catalyst, suggesting that the thiol and substrate compete for initial adsorption sites, possibly at the metal−support interface. These two methods were combined to evaluate the magnitude of the support effect on selective 4-methoxybenzyl alcohol oxidation. Correcting the catalytic activity of the catalysts to the number of sites determined by thiol titration provided clear evidence that the support has a strong influence on the catalytic activity of Au in benzyl alcohol oxidation.

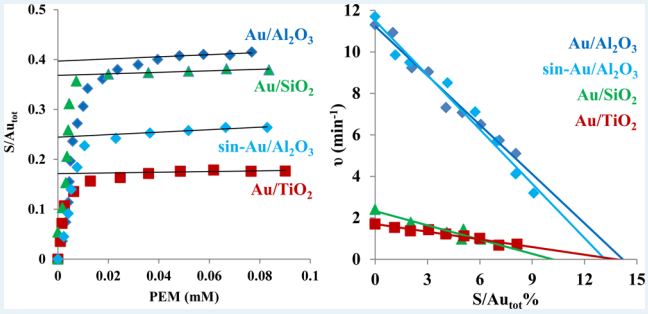

KEYWORDS: *gold catalysts, benzyl alcohol oxidation, support effects, kinetic poisoning, chemisorption, thiol adsorption, UV−visible spectroscopy*

INTRODUCTION

Supported Au catalysts show exceptional activity and/or selectivity at low temperatures in CO oxidation,[1,2] selective hydrogenations,[2,3] oxidations,[2,4,5] reductive coupling of nitro-aromatics,[6] and the water−gas shift (WGS) reaction.[2,7] Several factors have been suggested for the exceptionally high activity of Au catalysts, including quantum size effects,[8] particle geometry,[9,10] under-coordinated Au atoms,[11−14] and the role of the metal−support interface.[15] Despite the substantial research activity in gold-catalyzed oxidation reactions, the factors controlling catalytic activity are still not well understood.

The number of active sites is a critical measurement in heterogeneous catalysis. Transmission electron microscopy (TEM) provides important information on particle size and an estimate of the fraction of surface atoms; however, it struggles to detect the smallest metal nanoparticles and does not directly probe the number of active sites on a catalyst surface. Chemisorption is a desirable method because it provides a direct measure of the number of adsorption sites, samples a much larger number of particles, and, in many cases, can also be used to estimate particle size. There have been a few attempts to develop adsorption methods using low-temperature volumetric CO chemisorption[16−18] and methyl mercaptan adsorption monitored with gravimetry.[19] However, the reversible adsorption of CO on both Au and surface hydroxyl groups makes it difficult to differentiate chemisorption on Au from physisorption on the support, so no widely accepted chemisorption method exists for supported Au catalysts.

Although improved chemisorption techniques would benefit the quantification of Au catalysis, chemisorption data may not

Received: December 4, 2014
Revised: February 9, 2015
Published: February 19, 2015

DOI: 10.1021/cs501942t
ACS Catal. 2015, 5, 2232−2241

necessarily correlate with the number of active sites for a specific reaction. An alternate method for evaluating the number of active sites on a catalyst is through intentional poisoning or titration experiments. In these experiments, a controlled amount of poison is added to a catalyst and the resulting reduction in activity is monitored. Changes in the catalytic activity as a function of the amount of added poison may therefore shed light on both the number of active sites and any distribution in the inherent reactivity of the active sites. This general method has been applied to acid-catalyzed reactions over zeolites, using substituted pyridines[20,21] or Na vapor[22,23] as the active site titrant.

Fewer controlled poisoning studies have been applied to metal-based catalysts. Turkevich and co-workers developed a pulse poison/titration experiment using a variety of poisons to study ethylene hydrogenation over supported Pt catalysts in the 1970s.[24] More recently, Finke and co-workers evaluated the number of catalytic active sites on a 5% Rh/Al_2O_3 catalyst using CS_2 poisoning experiments.[25] Applying the same methodology to soluble polyoxoanion-stabilized Rh nanoparticles of comparable size allowed them to more precisely compare the inherent reactivity of the two catalysts on a per active site basis. Intentional poisoning experiments were also critical to identifying Rh_4 clusters (vs larger nanoparticles or mononuclear species) as the active catalysts in solution-phase Rh catalyzed benzene hydrogenation.[26] Buriak and co-workers also used CS_2 poisoning to compare monometallic Rh and bimetallic Pt−Rh hydrogenation catalysts.[27]

A few recent studies have used kinetic poisoning experiments to evaluate supported Au catalysts. The Kung group recently studied NaBr poisoning of Au/TiO_2 catalysts with a variety of X-ray absorption techniques and measured CO oxidation conversion.[16] We also studied NaBr poisoning of CO oxidation, performing a detailed kinetic analysis of the poisoned catalysts coupled with DFT calculations and infrared spectroscopy of adsorbed CO studies.[28] In an elegant study, the Katz group also used kinetic poisoning experiments of Au catalysts to show that different types of sites have markedly different activities for resazurin reduction.[29] Haider and co-workers performed a qualitative study using octadecanethiol and mercaptoacetic acid to poison benzyl alcohol oxidation.[30] Their results indicated conversion decreased in the presence of octadecanethiol but that the activity loss was markedly less when mercaptoacetic acid was used. The Medlin group has also shown that partially poisoning Pt and Pd catalysts with alkanethiols generally leads to decreased activity, but can also improve selectivity in some hydrogenation and hydrodeoxygenation reactions.[31−34]

The seminal work by Bain and co-workers showed thiols form self-assembled monolayers (SAMs) on gold surfaces.[35] This rich surface chemistry has been extensively studied and expanded[36] and led to the discovery that small gold nanoparticles could be prepared by reducing Au salts in the presence of thiols (the well-known Brust synthesis).[37] The resulting monolayer protected clusters (MPCs) have been similarly well-studied and utilized in a wide range of applications.[38,39] In this study, we sought to exploit Au−thiol chemistry to better understand the catalytic chemistry of Au. Specifically, we explored thiol adsorption as a method for evaluating the number of surface Au atoms in supported Au nanoparticle catalysts. We further extended this investigation to develop controlled thiol poisoning to estimate the number of active sites on several Au catalysts during 4-methoxybenzyl alcohol oxidation. The combination of these tests, along with appropriate characterization studies, allows for a more complete description of the substantial differences in activity from one catalyst to the next.

EXPERIMENTAL PROCEDURES

Materials and Instrumentation. Silica (Davisil, SA 430−500 m^2/g) was dried at 500 °C for 2 h before use. 1-Phenylethyl mercaptan (PEM) (>99%), 1-propanethiol (99%), 1-butanethiol (99%), 2-butanethiol (>98%), 2-methyl-2-propanethiol (99%), 1-hexanethiol (99%), 1-octanethiol (>98.5%), 1-dodecanethiol (>98%), triphenylphosphine (>98.5%), 4-methoxybenzyl alcohol (98%), and hexane (95+%, spectrophotometric grade) were purchased from Sigma-Aldrich and used without further purification. 1-Decanethiol (96%) was purchased from Alfa Aesar. $HAuCl_4$ was purchased from Strem Chemicals. Toluene (ACS grade) from Mallinckrodt Chemicals was dried over molecular sieves before use. AUROlite (approximately 1% Au/TiO_2 and 1% Au/Al_2O_3) catalysts were purchased from Strem Chemicals. The sintered Au/Al_2O_3 catalyst was heated under flowing H_2/N_2 (30% H_2, 140 mL/min) for 4 h at 500 °C. Water was purified to a resistivity of 17−18 MΩ·cm with an Elga Purelab Flex water purification system. Oxygen (5.0 grade) was purchased from Praxair and used without further purification.

UV−visible spectra were collected on a Hitachi U-2900 spectrophotometer. Quartz cuvettes (Fisher Scientific) were used for all of the UV−visible spectra. Gold elemental concentrations were determined with a Varian SpectrAA 220FS, using an acetylene/air flame as previously described.[40] Briefly, solid samples were placed in an Erlenmeyer flask, and freshly prepared aqua regia (2 mL) was added to the sample and allowed to digest at room temperature for 30 min. The sample was then heated slowly to 60 °C for 2 h, transferred to a volumetric flask (10 mL), diluted with nanopure water, and subsequently analyzed. Experimental errors for the method and the spectrometer are typically <5%.

X-ray Photoelectron Spectroscopy (XPS). XPS spectra were collected on a Kratos Analytical Axis Ultra DLD spectrometer, equipped with an Al Kα excitation source ($h\nu$ = 1486.6 eV), a 100 channel delay-line detector system, and a hemispherical sector analyzer. The powdered catalysts were finely ground using a mortar and pestle and pressed onto double-sided adhesive carbon tape. Loose particles were removed from the sample using nitrogen gas and then mounted on the sample holder of the XPS. The binding energy scale was calibrated by measuring the C 1s peak (BE = 284.9 eV). Survey scans were performed in the binding energy range of 0−1350 eV with a pass energy of 80. All spectra were analyzed using CasaXPS software.

Transmission Electron Microscopy (TEM). Au nanoparticles supported on the different supports were imaged using TEM. A small amount of powdered catalyst was dispersed in 10 mL of isopropanol and sonicated to obtain a uniform suspension. A tiny drop of this suspension was added to a lacey carbon-coated copper grid, and the grid was mounted onto the sample holder. Imaging was done using a field-emission JEOL 2010F microscope at an accelerating voltage of 200 kV and a probe current of 0.5 nA per nanometer. The instrument was operated in the STEM mode with high-angle annular dark field detectors. Analysis was performed using ImageJ software to count the number of Au particles and their individual diameters in approximately 20 images per catalyst to obtain the particle size distributions presented in the Supporting Information (SI).

Au/SiO_2 Catalyst Synthesis. About 750 mg of calcined SiO_2 was added to a round-bottom flask containing 15 mL of nanopure water, and 40 mL of 1.7 mM $HAuCl_4$ solution in nanopure water was added dropwise with continuous stirring. The mixture was then heated to 70 °C and maintained at that temperature for an hour. After the mixture had cooled to room temperature, 4 mL of 4 M ammonium hydroxide solution was added with constant stirring. After an hour, the solid was collected on a fritted funnel and washed four times with nanopure water; the filtrate was tested with $AgNO_3$ solution to ensure that the solid was free of chloride. The sample was dried overnight in a vacuum oven at 40 °C. The deposited gold was reduced under flowing H_2/N_2 (30% H_2, 140 mL/min) for 2 h at 200 °C and then cooled under

DOI: 10.1021/cs501942t
ACS Catal. 2015, 5, 2232−2241

flowing N_2. The catalyst was then transferred to a vial and stored in a dark refrigerator.

Thiol Adsorpton with Phenylethyl Mercaptan. Approximately 30 mg of catalyst was added to a centrifuge tube and washed twice with hexane by stirring, centrifuging, and decanting. Subsequently, 6 mL of hexane was added, stirred, and centrifuged; 4 mL of the supernatant solution was removed. Half of the removed supernatant was used as the UV−vis reference for the remainder of the experiment. The other half was used to measure a "zero" spectrum. The sample cuvette's solution was returned to the centrifuge tube, and 40 μL of 2 mM PEM in hexane was added, stirred for 1 min, and centrifuged for 5 min at 700 rpm. Next, 2 mL of the supernatant liquid was removed and a UV−vis spectrum was collected. The UV−vis sample solution was returned to the centrifuge tube, and this process (addition of PEM thiol and collection of UV−vis spectrum) was repeated >10 times. All experiments were perfomed at room temperature.

Benzyl Alcohol Oxidation Catalysis. A Wilmad Glasslab reactor (10 mL, 20−400 thread, 23 mm × 80 mm) with a septum-sealed cap was used for all reactions. The reactor was immersed in a water bath; reaction temperature was maintained using a Lauda-Brinkmann RM-6 recirculating heater pumping water through a copper coil immersed in the water bath. An Isotemp stirrer stirring at approximately 700 rpm was used to ensure a consistent temperature throughout the water bath. Oxygen was passed over the reaction mixture at atmospheric pressure. The catalysts were separately crushed and ground with a mortar and pestle. Solutions of 4-methoxybenzyl alcohol (0.1 and 2 M) were prepared gravimetrically.

Two methods were employed in the catalysis studies. In thiol pre-adsorption experiments, 5 mL of toluene, an appropriate amount of the thiol solution, and 15 mg of catalyst were added to the reactor, which was then placed in the water bath and heated to 50 °C under flowing O_2 with stirring at 700 rpm. After 10 min, 250 μL of 4-methoxybenzyl alcohol (2.0 M) in toluene was added via syringe to initiate the reaction. For competition experiments, a 10 mL aliquot of the 0.1 M substrate solution (1 mmol substrate) was added to the reactor, which was then placed in the water bath and heated to 50 °C under flowing O_2 with stirring at 700 rpm. After 10 min, the catalyst was weighed and added to the reactor to initiate the reaction.

Reactions were followed for 9−12 min; three to four aliquots (50 μL) were removed using a 1 mL pipet fitted with a Nalgene PTFE filter (0.45 μm). The samples were transferred to 2 mL GC sample vials containing 1 mL of dichloromethane (DCM) and analyzed by gas chromatography. Two injections were performed for every sample and manually integrated. Solution concentrations were determined from calibration curves prepared for the alcohol and aldehyde. Initial catalytic reaction rates were reported as moles of alcohol reacted per mole of Au_{total} per minute.

RESULTS AND DISCUSSION

Thiol Titration Method Development. There are few chemisorption methods that are appropriate for evaluating the fraction of Au surface atoms. We are aware of only a few attempts to use low-temperature volumetric CO chemisorption[16−18] and a report of methyl mercaptan adsorption using gravimetric analysis.[19] Gold−sulfur surface chemistry, however, is well-documented in the SAM literature.[36] Au−S bonds are strong (on the order of 50 kcal/mol),[36] so it should be possible to use thiols to titrate Au surface sites and provide a measure of the fraction of exposed surface atoms in Au catalysts. The previous measurement used a relatively toxic adsorbate (methyl mercaptan) and gravimetric detection, which is not readily available in many research laboratories, suffers from buoyancy effects, and may not be as relevant for liquid-phase reactions.[19] To overcome these challenges, we developed a simple biphasic UV−vis spectroscopic method to evaluate the fraction of surface Au atoms.

To use UV−vis spectroscopy, the thiol adsorbate should be relatively nonvolatile and have an absorption band in the UV−vis region. The $\pi-\pi^*$ transitions associated with aromatic compounds are well-known to fall in this range, so we investigated PEM as a potential titrant. This molecule has the additional advantage of having the phenyl ring somewhat removed from the sulfur atom, which should minimize steric interactions between thiols adsorbed on the surface. The UV absorption of PEM (240−270 nm, SI) is far in the UV, so the solvent needed to be both UV transparent and nonpolar to dissolve the PEM. After a number of preliminary experiments, we settled on *n*-hexane as an appropriate solvent.

The $\pi-\pi^*$ HOMO−LUMO transition in the UV spectrum of PEM (SI; Figure 1) has five distinct vibrational bands in the

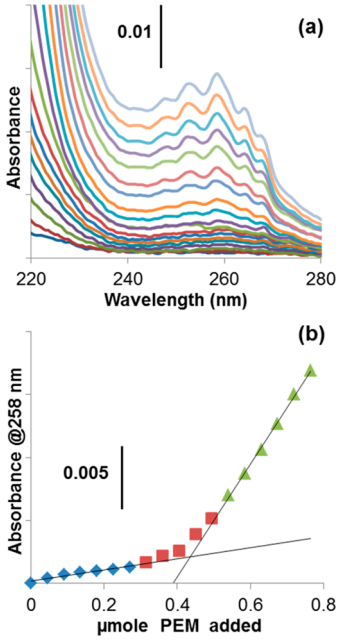

Figure 1. (a) UV−vis spectra during the titration of Au/Al_2O_3 (30 mg) suspended in hexane with PEM. (b) Titration plot following absorbance at 258 nm in panel a as a function of added PEM.

240−280 nm region, with the band at 258 nm being the most pronounced. The molar absorptivity at 258 nm (ε_{258} = 220 ± 7 Abs/M/cm) was determined from calibration curves, which were always linear at the concentrations used. Control titration experiments with several supports (Al_2O_3, SiO_2, and TiO_2) were well-behaved and showed no PEM adsorption, at least to the detection limits of our method (titration plots are available in the SI). Two experimental difficulties were encountered in developing the titration method with supported catalysts. First, as the titration of the catalyst progressed, there was a gradual shift in the baseline, most likely due to the gradual desorption of residual organics absorbed on the catalyst. Washing the catalyst twice with *n*-hexane prior to beginning was critical to obtaining high-quality data. Additionally, there is an overall increase in absorbance due to a more intense higher energy transition (below 240 nm). To account for this, we corrected the baseline of each spectrum at 273 nm; that is, the absorbance at 273 nm was subtracted from the absorbance at 258 nm to determine the absorbance due to the $\pi-\pi^*$ HOMO−LUMO transition of PEM.

Thiol Adsorption Results. The UV−vis spectra collected in the titration of Au/Al_2O_3 with PEM and the resulting plot of

DOI: 10.1021/cs501942t
ACS Catal. 2015, 5, 2232−2241

Abs_{258} versus micromoles of PEM added are shown in Figure 1. There is only a small increase in absorbance until approximately 0.3 μmol of PEM has been added, indicating essentially all of the PEM added in this early stage of the titration adsorbs onto the gold. At the later stages of the titration, the slope of the line in Figure 1b corresponds to the molar absorptivity of PEM, indicating that all of the PEM added at this stage is free in solution. Similar spectra and titration plots were obtained for the Au/TiO_2 and Au/SiO_2 catalysts; these can be found in the SI.

The titration plot shown in Figure 1 is the most direct presentation of the experimental data. Using the PEM molar absorptivity to determine the equilibrium concentration of thiol in solution at each point, it is also possible to present the data as a traditional Langmuir adsorption isotherm (Figure 2a). The data can also be examined as a Langmuir plot, as we have done for CO adsorption on Au.[41−43] Each of these methods can be used to determine an end point for the titration; as Table 1 shows, for a given catalyst, the three methods give essentially the same result. In the following discussion, we prefer to use the Langmuir plot (Figure 2b) because it uses the data points that have the smallest intrinsic experimental errors and extrapolates to a maximum adsorption value. The Langmuir plot also yields a value for the adsorption equilibrium constant at the end of the titration, which allows for comparisons between catalysts.

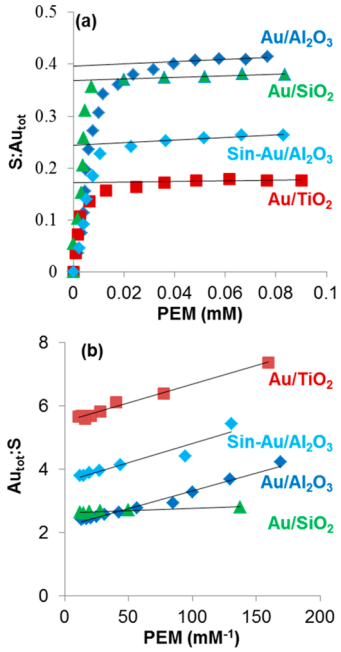

Figure 2. (a) PEM adsorption isotherms at 22 °C for the four catalysts determined via UV−visible spectroscopy and (b) Langmuir plots from the data in panel a. The *y*-intercepts in the plots represent the experimental determination of the total number of thiol-binding sites. Thiol-binding constants were determined from the slope and intercepts in panel b.

Adsorption isotherms and Langmuir plots for the four catalysts are shown in Figure 2; the extracted values are combined in Table 1. The binding constants for PEM to the Au/TiO_2 and Au/Al_2O_3 catalysts are essentially the same. Furthermore, the consistency of the equilibrium constant before and after sintering of the Au/Al_2O_3 catalyst suggests that, at least for this support, any particle size effect on the thiol-binding energetics is relatively small.

In a comparable study, Karpovich and Blanchard used adsorption/desorption kinetics to investigate Au−thiol binding from hexane and cyclohexane solution.[44] Using a model system composed of polycrystalline Au (primarily Au (111)) vapor deposited onto a quartz crystal microbalance, they measured binding constants for 1-octadecanethiol ($\sim 1 \times 10^4$ M^{-1}) and 1-octanethiol ($\sim 2 \times 10^3$ M^{-1}).[44] These values are somewhat lower than our values for PEM on Au catalysts, possibly due to the differences between small nanoparticles and extended Au surfaces.[44] Ravi et al. recently reported a detailed isothermal titration calorimetry (ITC) study of carboxylic acid terminated alkanethiol binding to citrate-stabilized Au NPs.[45] Their studies showed that the thiol-binding constant was largely independent of both chain length and nanoparticle size, in good general agreement with our results; however, their binding constants ($\sim 10^6$−10^7 M^{-1}) were about an order of magnitude greater than our measured values. Ansar et al. similarly used surface-enhanced Raman spectroscopy to investigate mercaptobenzimadazole adsorption on 13 nm citrate-stabilized Au particles.[46] Their values showed a slight pH dependence, but were in the same range as those measured by Ravi et al. It is not surprising that these measurements differ somewhat from ours and those by Karpovich and Blanchard.[44] Ravi et al. measured both the differential heat of adsorption and the adsorption equilibrium constant for the net thiol binding and displacement of citrate from the nanoparticle surface. Our measurements immobilize the thiol from solution onto a solid, which may carry a substantial entropic penalty and will be further convoluted by solvation−desolvation processes. Given the differences in the experiments, the differences in the binding constants between the two methods are reasonable. Because the support effects for the Au/Al_2O_3 and Au/TiO_2 catalysts are small, this method appears to provide a reasonably direct measure of the binding constant and adsorption energy of thiols on Au nanoparticles.

Table 2 shows TEM and PEM adsorption data for the four catalysts. Representative TEM micrographs and particle size

Table 1. PEM Adsorption at 22 °C on the Series of Supported Au Catalysts Used in This Study

		S/Au_{total} (mol %)				
catalyst	Au wt %	titration plot[a]	extrapolated to [PEM] = 0[b]	Langmuir plot[c]	K_{eq} (M^{-1}) × 10^5	ΔG_{ads} (kJ/mol)
Au/TiO_2	0.88	19 ± 1	17 ± 1	18 ± 1	4.7 ± 0.2	−32 ± 1
Au/Al_2O_3	0.81	42 ± 1	40 ± 1	45 ± 1	2.0 ± 0.1	−30 ± 1
sin-Au/Al_2O_3	0.81	27 ± 1	25 ± 1	28 ± 1	3.0 ± 0.4	−31 ± 1
Au/SiO_2	1.21	39 ± 1	37 ± 1	38 ± 1	20 ± 2	−36 ± 1

[a]S/Au ratio determined from the intersection of the two lines shown in Figure 1b. [b]S/Au ratio determined from extrapolation of the linear adsorption region to zero thiol concentration as shown in Figure 2a. [c]S/Au ratio determined from the slope of the Langmuir plot as shown in Figure 2b.

DOI: 10.1021/cs501942t
ACS Catal. 2015, 5, 2232−2241

Table 2. TEM Particle Size and Au:S Surface Stoichiometry Data

	TEM		
catalyst	d_{av}[a] (nm)	% Au_{surf}[b]	Au_{surf}:S[c]
Au/TiO_2	2.9 ± 0.9	40	2.2 ± 0.7
Au/Al_2O_3	<2	>60	
sin-Au/Al_2O_3	2.2 ± 0.7	53	2.0 ± 0.7
Au/SiO_2	3.5 ± 0.7	33	0.9 ± 0.3

[a]Particle size distributions available in the SI. [b]Au_{surf} fraction (i.e., dispersion) determined from average TEM particle size using D = 1.16/d(nm). [c]Au_{surf}:S is the stoichiometry for the number of surface Au atoms per adsorbed thiol, determined from PEM titration and TEM data (TEM data are available in the SI).

distributions are available in the SI. Comparing titration data to TEM measurements is important in the evaluation of whether the titration method is useful for evaluating particle size. The Au/Al_2O_3 catalyst had particles that were too small to image with TEM; thus, the thiol titration (Table 1) provides the only determination of the amount of surface Au in the catalyst. To better evaluate the Au−S surface stoichiometry, we sintered the Au/Al_2O_3 catalyst (sin-Au/Al_2O_3) to increase the Au particle size. The Au_{surf}:S ratio calculated from the titration and TEM data for sin-Au/Al_2O_3 is essentially the same as the Au/TiO_2 catalyst (about 2). This suggests that this value, which corresponds to thiols adsorbed in a bridging configuration on a pair of Au sites, is a reasonable surface stoichiometry to use for highly dispersed catalysts. The measurement errors in the PEM titration are on the order of 5%, so the "imprecision" in the Au_{surf}:S ratios is almost exclusively due to the intrinsic particle size distributions, which are on the order of 20−30%. Assuming the Au_{surf}:S ratio remains at ∼2 for the Au/Al_2O_3 catalyst, the thiol adsorption experiment estimates the metal dispersion to be about 85%, suggesting particles are on the order of 1 nm.

A brief discussion of the Au_{surf}:S ratios in the thiol-stabilized nanoparticle and SAM literature is warranted to place our results into the proper context. Reported ratios in the literature vary greatly, which is likely due to the specifics of how the Au_{surf}:S ratio is determined. Molecular Au clusters with well-defined metal−ligand ratios are the most straightforward place to start. Specific examples include $Au_{20}(SCH_2CH_2Ph)_{16}$,[47] $Au_{36}(SCH_2CH_2Ph)_{24}$,[48] $Au_{102}(S-C_6H_4-COOH)_{42}$,[49] and several phosphine-stabilized cationic Au clusters.[50] The smallest of these systems have Au_{surf}:S ratios at or near unity, which is likely the lowest value expected for a supported catalyst. As the clusters become larger, the Au_{surf}:S ratio increases to around 1.3.

Much of the SAM literature on extended surfaces and larger nanoparticles is more complicated. The thiol packing density depends on several factors, including the exposed Au crystal facet; however, several results suggest that thiols preferentially adsorb in three-fold hollow sites, yielding a Au_{surf}:S ratio of 3.[51] Our results are between these two limiting cases, but a number of other studies, particularly computational work, suggest that bridging sites (Au_{surf}:S = 2) have stability similar to that of 3-fold hollow sites.[52−56] The literature on Au_{surf}:S ratios for nanoparticles in solution, nominally 2−50 nm, varies and is therefore difficult to compare to our results. Some studies show that the Au_{surf}:S ratio varies substantially with particle size,[57−59] whereas others have observed little or no particle size dependence.[60−62]

The Au/SiO_2 catalyst has two important distinctions relative to the other catalysts: (i) the PEM binding constant is a factor of 3 higher and (ii) the Au_{surf}:S ratio is close to 1 rather than 2. Control experiments showed no thiol adsorption on the silica support, and the adsorption thermodynamics are consistent with thiol binding to Au. Given the overall quality of the adsorption data, the difference in PEM binding thermodynamics is likely meaningful. We also note that the Langmuir plots use the last several points of the titration (generally 6−10), so the determined binding constants are for thiol adsorption to a nearly saturated Au surface. Adsorption equilibrium constants at lower coverages may be larger, as steric repulsions and changes in surface electronics are expected to reduce adsorption energies at high coverages. However, these trends run counter to our observations with the Au/silica catalyst: namely, this catalyst has the largest particles yet it generates the highest thiol surface coverage and a slightly larger thiol-binding energy. This suggests a slightly different chemical interaction between the thiols and the Au surface on the Au/SiO_2 catalyst.

One possibility is that the Au_{surf}:S ratio is substantially different due to the nature of the support and/or the metal−support interactions. Silica is far more acidic (isoelectric point (IP) ∼ 2) than either titania or alumina (IP values of ∼6 and ∼8, respectively),[63] so considering the effects of greater hydronium availability is a reasonable starting point. Several studies from the SAM and solution-phase NP literature suggest that thiol binding is preceded by proton loss to generate a thiolate.[36,58,64−66] Thiolate binding may then be partially limited by the presence of hydronium, which is necessary to balance the surface charge associated with the thiolates. Silica, being substantially more acidic than the other two supports, should have much higher surface hydronium concentrations capable of serving this purpose, possibly allowing for greater thiol densities on Au.

Another possibility is that the more acidic silica surface helps to catalyze thiol oxidation to disulfides on the Au surface. This is a facile reaction that is ubiquitous in biological chemistry, as disulfide bridges play a multitude of roles in biological chemistry, particularly the structure of proteins.[67−69] Additionally, the industrial Merox process employs a cobalt phthalocyanine complex at nearly ambient temperatures to convert thiols to disulfides as a means of sweetening crude oil.[70] Although not common, there have been reports of thiols adsorbing to Au surfaces as disulfides.[66,71] Au is an excellent low-temperature oxidation catalyst that can abstract hydrides from oxidizable atoms.[72] Furthermore, Au is active in other heteroatom coupling reactions[6] and, in the presence of water and hydronium, is capable of forming Au-bound peroxides near the metal−support interface.[15] Thus, the chemistry of disulfide formation is reasonable at room temperature on this catalyst; however, further investigations are required to understand why this support differs from the nonacidic oxides.

Finally, the higher thiol surface coverage might be explained by the presence of either unreduced Au or very small particles that are unobservable by TEM.[73] This seems unlikely, however, because the particle size distribution would have to be extraordinarily bimodal for this model to be realistic. Although linear Au(I) complexes binding two ligands are well-known, one-third to half of the Au would have to be present as Au(I) to account for the Au_{surf}:S ratio measured by UV titration. XPS data for this catalyst (see the SI) shows no evidence of Au(I), so this possibility can be discounted.

DOI: 10.1021/cs501942t
ACS Catal. 2015, 5, 2232−2241

These studies also provide insight into the interactions between S and Au in SAMs and thiol MPCs, because the Au NPs are stabilized against agglomeration through strong bonds with the oxide support. Thus, the remaining surface is exposed and devoid of capping agents, which may affect measurements associated with S−Au interactions. In particular, the nature of the Au−S bonding has been debated, particularly the oxidation states of the two species and the fate of the proton.[36,74−76] Recent work by Matthiesen and co-workers provided strong evidence for the production of H_2 during thiol binding, as Kankate et al. have observed in UHV studies.[77] In many instances, loss of hydrogen is presumed to coincide with oxidation of the Au surface to balance the thiolate charge.[64,75−77]

To address this, and to evaluate how adsorbed thiols might change Au surface chemistry, we performed XPS studies, specifically looking for changes to Au oxidation state due to thiol adsorption. Figure 3 shows the Au 4f region for the Au/TiO_2 catalyst with and without adsorbed thiols; data for the Au/Al_2O_3 and Au/SiO_2 catalysts can be found in the SI. Thiol adsorption induces a slight Au core electron shift toward weaker binding energy, consistent with increased electron density on the Au. This suggests that thiol adsorption is, on balance, an electron-donating interaction; there is no indication of Au oxidation. Unfortunately, the thiol loadings were too low to observe changes to the S oxidation state. However, the XPS data provide no evidence for the oxidation of Au upon thiol adsorption, which suggests the thiolate is more likely to be oxidized. The XPS data for the Au/SiO_2 catalyst (available in the SI) showed no shift in the Au 4f binding energies upon thiol adsorption, suggesting that the thiols are less electron donating when adsorbed on this catalyst. This is consistent with some degree of thiol oxidation to disulfides (vide supra).

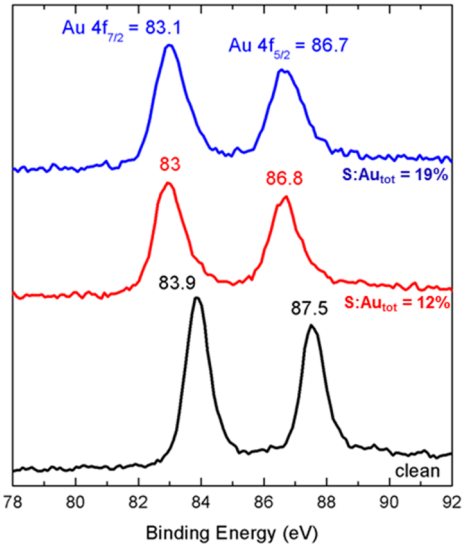

Figure 3. Au 4f spectra of clean and 1-butanethiol-covered Au/TiO_2 catalysts ($S:Au_{total}$ ratios are shown below the spectra). Peak positions were corrected to the C(1s) peak (284.9 eV). Spectra are offset for clarity.

Kinetic Thiol Titrations. Kinetic titrations, in which catalytic activity is intentionally diminished through the addition of controlled amounts of a strong poison, potentially allow researchers to evaluate and compare the number of active sites in catalytic materials.[28,78] As shown above, thiol adsorption onto Au catalysts is readily quantifiable, so it is plausible that thiols might be useful as titrants to estimate the number of active sites responsible for the observed catalytic activity. We examined the aerobic oxidation of 4-methoxybenzyl alcohol over Au/TiO_2, Au/Al_2O_3, and Au/SiO_2 catalysts to test this hypothesis and to evaluate the influence of the support on catalytic activity. Benzyl alcohol oxidation over Au is an ideal test reaction because the reaction is highly selective for the aldehyde at low conversion and a key step in the reaction mechanism has been identified. Substantial mechanistic evidence points to a hydride transfer from the benzylic carbon to the Au nanoparticle as the rate-determining step,[72,79,80] so the reaction is potentially sensitive to changes in the Au induced by the varying interactions with the support. Furthermore, the reaction is rapid at moderate temperatures, facilitating the use of initial rate experiments. In these measurements, conversions were always <12% (typically <5%), and 4-methoxybenzaldehyde was the only product observed. Plots of conversion versus time were always linear; the slopes of these lines were used to determine the initial rate of each experiment.

Figure 4 shows the results from a series of kinetic titration experiments using 1-butanethiol to poison the Au/Al_2O_3 catalyst. Each data point in the figure is the result of a separate poisoning experiment in which the initial reaction rate was determined. The plot shows two clear regions. At low thiol concentrations (blue data points), the rate decreases linearly with added thiol. After the addition of about 10% thiol (relative to total Au), the data deviate from this trend (maroon data points); additional thiol becomes a less effective poison. This tailing effect was consistently observed for all of the catalysts using several different thiols and has been observed in kinetic poisoning studies of different systems.[26,78]

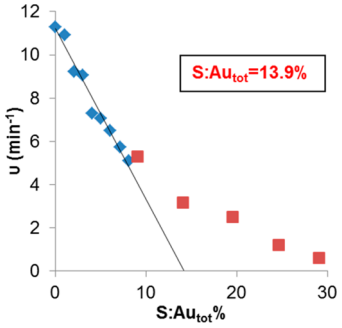

Figure 4. Representative kinetic titration plot for Au/Al_2O_3. The plot shows the decrease in measured 4-methoxybenzyl alcohol oxidation activity as the concentration of 1-butanethiol in the reaction mixture increases. The *x*-intercept represents the experimental determination of the number of active sites, expressed as the number of thiols bound per total Au in the catalyst.

This result is somewhat surprising. Steric crowding on the surface would likely limit substrate access to the Au and therefore increase (not decrease) the poisoning effectiveness at high thiol coverage. One reasonable explanation is that there is a range in the inherent activity of the catalyst active sites and that the thiols bind most strongly to (and poison) the most active sites first. Our UV titration is not sufficiently sensitive to monitor the low solution concentrations (<10 μM) of thiol required to examine potential differences in thiol-binding strength as a function of coverage, so we cannot directly

DOI: 10.1021/cs501942t
ACS Catal. 2015, 5, 2232−2241

evaluate this. It is also important to point out that all of the S:Au_{total} ratios shown in Figure 4 are in the strong thiol-binding regime of the adsorption isotherm in Figure 2. It therefore seems unlikely that the tailing in Figure 4 is due to large differences in thiol-binding strength as a function of coverage. It is also possible that thiols bind to the active site first, but diffuse to nonactive (or low activity) sites at higher S coverages. Even if Au−S bond strengths are slightly lower away from the active site, the thermodynamic driving force of the additional Au−S bond appears to be more than sufficient to overcome this difference. Thus, the poisoning is likely to occur primarily through a site-blocking mechanism.

Regardless of the origins of the tailing at higher thiol concentrations, it was consistently present and should be accounted for in using the poisoning data. We chose to use the extrapolation of the linear poisoning regime (blue data in Figure 4) to the *x*-intercept as a metric related to the number of active sites. This is the same method that Finke and co-workers have used in their studies of Rh-catalyzed reactions.[26,78] The value might be most appropriately interpreted as an estimate of the number of high-activity sites. Additionally, the poisoning values obtained with this method are in reasonable agreement with Haider and co-workers' more qualitative poisoning study using octadecanethiol.[30] Other poisoning models might also work, particularly a weak adsorption model;[81] however, we prefer the simpler linear model as an initial estimate as it is straightforward, easy to understand, and easily transferrable between different catalysts and thiols.

As Finke and co-workers have outlined,[78] and we have previously argued,[28] this method inherently assumes a poison:active site ratio of 1:1. It is difficult to evaluate the validity of this assumption, however, particularly because the Au_{surf}:S ratio determined in the titration experiment was different for the Au/SiO_2 catalyst. This highlights an important difference between the two measurements. The UV−vis thiol adsorption experiments probe the surface stoichiometry at maximum thiol coverage, whereas the kinetic poisoning experiments evaluate how much thiol is required to eliminate catalytic activity. It is unclear if these two are related, particularly because the kinetic poisoning experiments show that the initial thiol adsorption sites appear to be responsible for the catalysis. If the poison:active site ratio is different for the Au/SiO_2 catalyst, it introduces a systematic determinate error in the interpretation of the "true" turnover frequency for this catalyst. However, because our primary goal is to compare the relative number of active sites across catalysts, the possibility of a determinant error should have a consistent effect on the resulting TOFs and should not substantially influence our comparisons.

In developing this technique as a method for evaluating the number of catalytic sites, we had two additional concerns: (i) the thiol chain length and steric crowding on the Au surface might affect the extrapolated value, and (ii) competition between the thiol and the substrate (4-methoxybenzyl alcohol, the concentration of which is orders of magnitude higher than the thiol) might influence the poisoning. We addressed these issues by (i) varying the thiol chain length and (ii) changing the point in the experiment in which thiols were introduced to the system. These experiments are compiled in Figure 5 and Table 3. In the first set of experiments (Figure 5a), we varied the thiol chain length, adding the thiol at the beginning of the experiment, before the substrate was added. This allowed the thiol to fully adsorb to the catalyst before the substrate was introduced.

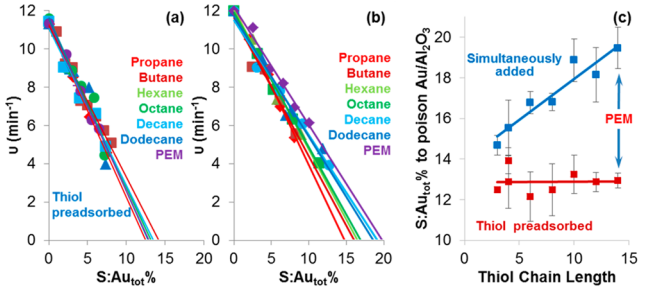

Figure 5. Effects of thiol chain length and order of addition on 4-methoxybenzyl alcohol oxidation catalyzed by Au/Al_2O_3: (a) thiol is allowed to interact with the catalyst before substrate introduction; (b) thiol and substrate are added to the reaction mixture simultaneously. Panel c shows the intercepts from panels a and b plotted against thiol chain length.

Table 3. Thiol Kinetic Poisoning Data of 4-Methoxybenzyl Alcohol by Au/Al_2O_3

	S:Au_{total}% for kinetic poisoning[a]	
catalyst poison	thiol preadsorbed before reaction	substrate and thiol added simultaneously
1-propanethiol	12.5 ± 0.2	14.7 ± 0.5
1-butanethiol	13.9 ± 0.6	15.5 ± 1.4
2-butanethiol	14.0 ± 0.3	14.7 ± 1.4
2-methyl-2-propanethiol	12.9 ± 1.3	13.0 ± 0.8
1-hexanethiol	12.1 ± 1.2	16.8 ± 0.5
1-octanethiol	12.5 ± 1.3	16.8 ± 0.4
1-decanethiol	13.3 ± 0.9	18.9 ± 1.1
1-dodecanethiol	12.9 ± 0.5	18.2 ± 1.3
PEM	12.9 ± 0.4	19.5 ± 1.0
triphenylphosphine	10.1 ± 0.3	11.6 ± 0.5

[a]Standard deviations calculated from averages of at least three trials.

The kinetic poisoning values (about 13% S:Au_{total}) were extremely consistent with this method and in good agreement with Haider and co-workers' limited octadecanethiol poisoning study.[30] PEM, a secondary thiol (2-butanethiol), and even a tertiary thiol (2-methyl, 2-propanethiol) also yielded similar kinetic poisoning values, suggesting surface crowding is relatively unimportant in determining the number of active sites. Indeed, it takes a very large poison such as triphenylphosphine (Table 3) to induce a substantial deviation from the consistent value in the preadsorption study. The curvature inherently associated with smaller particles likely decreases steric repulsions relative to a flat surface, making steric effects less important for smaller particles.[36]

We also examined adding the thiol simultaneously with the substrate by initiating the reaction by adding the catalyst (Figure 5b). Two noteworthy conclusions can be drawn from these data. First, under these conditions, there is a clear trend in poisoning effectiveness with chain length. Second, the *x*-intercepts of the plots in Figure 5b are shifted to larger S:Au_{total} values, indicating greater amounts of thiol are required to poison the most active sites on the catalyst. This was true for all of the thiols tested (see Figure 5c). This suggests the substrate and thiols do indeed compete for active sites under these conditions, with longer chain thiols being less able to access the Au active sites. This is somewhat surprising, as one would not expect the order of addition to substantially affect the thermodynamics and competition for Au active sites. We

DOI: 10.1021/cs501942t
ACS Catal. 2015, 5, 2232−2241

note that all of these poisoning titration values are well within the strong adsorption regime of the UV−vis studies (Figure 2). This suggests that the difference between the two types of thiol addition experiments is probing a subtle aspect of the reaction mechanism, not differences in thiol-binding strength.

At present, we believe the best explanation for the differences in activity based on when the thiol is added are that the most active sites are at the Au-support interface and that proton abstraction from the thiol is required for the most effective poisoning. First, thiolates are stronger ligands and therefore better poisons for Au and are often considered to be the primary stabilizers in thiol-protected Au nanoparticles.[36,58,64−66] This is most likely to occur at the metal−support interface, where the proton can be transferred to a support hydroxyl group or adsorbed water. Our previous work has shown that the proton transfer properties of even small amounts of adsorbed water can play a critical role in catalytic reactions.[15] Transfer to adsorbed water in particular would create a highly mobile hydronium ion that could rapidly balance and spread charge across the catalyst surface, including the charges associated with thiolates adsorbed on the Au.[15,82] Ansar et al. showed the addition of organothiols to aqueous Au colloids and Au powder rapidly releases protons and that the number of protons released is proportional to the amount of thiol adsorbed onto the Au surface.[75] Corma's mechanism for benzyl alcohol oxidation proposes loss of a proton to form an alkoxide that binds to the Au, although there is no description in the mechanism of where the proton ends up.[72] The small amount of thiols needed for kinetic poisoning relative to total thiol adsorption is consistent with the conclusion that thiols initially adsorb to Au at the metal−support interface where binding to Au can be accompanied by thiol deprotonation; the resulting thiolates then may migrate along the Au particle until the surface is saturated with thiols.

Thiol deprotonation also provides a framework for understanding the differences between preadsorbed and simultaneously added thiols. When the thiol is preadsorbed, the support surface is fully accessible and proton transfer occurs unfettered, giving the best estimate for the number of highly active sites. When thiol and benzyl alcohol are added simultaneously, thiols must compete with benzyl alcohol for initial access to the support hydroxyls or adsorbed water at the metal−support interface, so that deprotonation can accompany thiolate−Au binding. This is reasonable because the alcohol groups on benzyl alcohol are likely to interact with the support through H-bonding interactions, and the substrate concentration is roughly 1000 times greater than the poison. Adsorption experiments monitored by gas chromatography confirm that benzyl alcohol binds to the titania and alumina supports in large quantities (see SI).

Given the likely deprotonation chemistry and the understanding that strong Au−S bonding still provides the thermodynamic driving force for the adsorption process, the relatively small differences in the poisoning effectiveness for small thiols seems reasonable. This also explains the trend in reduced poisoning effectiveness with chain length: the longer chain thiols are increasingly hydrophobic and have a more difficult time accessing the more polar support. All of these data further support the conclusion that the reaction occurs at or near the metal−support interface, as benzyl alcohol adsorption on the support would help hinder thiol adsorption at these interfacial sites.

Evaluating Particle Size and Support Effects on Au Catalysts. The Au/Al_2O_3, sin-Au/Al_2O_3, Au/TiO_2, and Au/SiO_2 catalysts have substantial differences in activity for benzyl alcohol oxidation, with the Au/Al_2O_3 catalysts being nearly an order of magnitude more active on a per total Au basis. Quantifying these activity differences on a per active site basis is the first step to understanding the origins of these rate differences. Figure 6 shows the kinetic titration results for the four catalysts; these data are compared with other characterization data in Table 4. The kinetic poisoning titrations for these catalysts are similar, suggesting around 12% of the total Au is active. For all of the catalysts, this value is lower than the total PEM adsorption measured in the UV−vis titration, indicating that some of the surface Au atoms are active for the reaction. These are likely the atoms at or near the metal−support interface. On the basis of the average particle sizes, roughly 4−8% of the total Au atoms are strictly at the interface between the nanoparticle perimeter and the support. Given the size of the alcohol and that the hydride abstraction from the benzylic carbon likely occurs an angstrom or two away from the alcohol group, it seems reasonable that atoms near and not strictly at the metal−support interface would likely be capable of acting as a hydride acceptor during the reaction. Thus, a value of 12% of the total Au for the number of active sites appears to be relatively consistent with the catalytic activity occurring near the support. This conclusion is also consistent with the differences in poisoning found with the timing of thiol addition as discussed above.

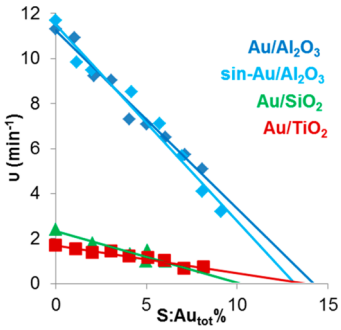

Figure 6. Kinetic titrations of 4-methoxybenzyl alcohol oxidation activity with 1-butanethiol for Au/Al_2O_3, sin-Au/Al_2O_3, Au/SiO_2, and Au/TiO_2.

The large differences in TOF indicate that the support plays a substantial role in affecting the benzyl alcohol oxidation activity of Au. This proof-of-concept study is not designed to address the nature of the support effects on this reaction, so a detailed discussion of its origin is not warranted. The poisoning experiment does, however, provide a direct and straightforward means of measuring these effects and allows for an initial evaluation of the potential magnitude of any support-induced geometric and/or electronic effects.

Similarly, this study was not designed to fully examine potential particle size effects on this reaction. Sintering of the Au/Al_2O_3 catalyst has the expected effect of increasing the particle size, decreasing the total PEM adsorption, and slightly decreasing the number of active sites (estimated by kinetic titration). At the same time, both the total activity and the activity per active site increased slightly upon sintering. This indicates that larger particles are more active for this reaction, as has been suggested previously.[30] A more detailed study

DOI: 10.1021/cs501942t
ACS Catal. 2015, 5, 2232−2241

Table 4. Kinetic Poisoning (1-Butanethiol) and PEM Adsorption Results for Au/TiO_2, Au/SiO_2, Au/Al_2O_3, and sin-Au/Al_2O_3

catalyst	rate (min^{-1}/Au_{total})	TEM d_{av} (nm)	UV titration $S:Au_{total}$%	kinetic titration $S:Au_{total}$%	TOF min^{-1}/site
Au/TiO_2	1.7 ± 0.2	2.9	18 ± 1	13.3 ± 0.8	13 ± 2
Au/SiO_2	2.4 ± 0.3	3.5	38 ± 1	9.5 ± 1.0	25 ± 4
Au/Al_2O_3	11.4 ± 0.5	<2	43 ± 1	13.9 ± 0.6	82 ± 5
Sin-Au/Al_2O_3	11.7 ± 0.5	2.2	27 ± 1	12.9 ± 0.6	91 ± 6

examining these particle size and support effects is currently underway.

CONCLUSION

UV−vis spectroscopy was used to follow PEM adsorption from hexane solution, thus providing a means for evaluating the total amount of surface Au available. Test Au/Al_2O_3 and Au/TiO_2 catalysts showed very similar behavior in PEM titrations, having essentially the same thiol-binding constants and surface stoichiometry (Au_{surf}:S) of ∼2. Despite having a significantly higher surface thiol coverage (Au_{surf}:S ∼ 1), the Au/SiO_2 catalyst had a somewhat stronger thiol-binding constant.

We also developed a method for evaluating the number of benzyl alcohol oxidation active sites by intentionally adding small amounts of thiol to the reaction mixture. For all of the thiols and catalysts tested, catalytic activity initially decreased linearly with thiol addition, but then tailed off. Extrapolating the linear portion of the plot to zero activity represents the best method for estimating the number of active sites on the catalyst.

When the thiol was added before the benzyl alcohol substrate, the extrapolated titration end point was independent of thiol chain length; even secondary and tertiary thiols gave the same poisoning value. However, when the thiol and benzyl alcohol substrate were added simultaneously, longer, more hydrophobic thiols were less effective poisons. This change is likely due to a competition between the substrate and thiol for support hydroxyl sites or adsorbed water located at the metal−support interface, suggesting thiol poisoning likely requires proton loss. Furthermore, the kinetic titration values were substantially lower than the total PEM adsorption measured by UV spectroscopy. Together, these data suggest that the key hydride transfer step likely occurs at or near the metal−support interface.

Kinetic poisoning studies showed the Au/TiO_2 and Au/Al_2O_3 catalysts had similar active site concentrations. Interestingly, sintering the Au/Al_2O_3 catalyst, which originally had particles too small to observe by TEM, had only a small effect on the number of active sites. Correcting the catalytic activity of the catalysts for the number of thiol titration sites provided clear evidence that the support has a strong influence on the catalytic activity of Au in benzyl alcohol oxidation.

ASSOCIATED CONTENT

Supporting Information

The following file is available free of charge on the ACS Publications website at DOI: 10.1021/cs501942t.

Figures S1−S14, Tables S1 and S2, and experimental details of catalytic experiments (PDF)

AUTHOR INFORMATION

Corresponding Author

*(B.D.C.) E-mail: Bert.chandler@trinity.edu. Phone: (210) 999-7557. Fax: (210) 999-7569.

Notes

The authors declare no competing financial interest.

ACKNOWLEDGMENTS

We gratefully acknowledge the U.S. National Science Foundation (CBET-1160217 and CHE-1012395) and the Welch Foundation (Departmental Grant W-0031) for financial support of this work. A.M. and R.M.R. acknowledge the Department of Energy, Office of Basic Energy Sciences, Chemical Sciences, Geosciences, and Biosciences Division, Catalysis Sciences Program, under Grant DE-FG02-12ER16364 for partial funding of this research. We thank Leslie Cook for performing benzyl alcohol adsorption experiments.

REFERENCES

(1) Saavedra, J.; Doan, H. A.; Pursell, C. J.; Grabow, L. C.; Chandler, B. D. *Science* **2014**, *345*, 1599−1602.
(2) Takei, T.; Akita, T.; Nakamura, I.; Fujitani, T.; Okumura, M.; Okazaki, K.; Huang, J.; Ishida, T.; Haruta, M. *Adv. Catal.* **2012**, *55*, 1−126.
(3) Corma, A.; Serna, P. *Science* **2006**, *313*, 332−334.
(4) Zope, B. N.; Hibbitts, D. D.; Neurock, M.; Davis, R. J. *Science* **2010**, *330*, 74−78.
(5) DellaPina, C.; Falletta, E.; Rossi, M. *Chem. Soc. Rev.* **2012**, *41*, 350−369.
(6) Grirrane, A.; Corma, A.; Garcia, H. *Science* **2008**, *322*, 1661−1664.
(7) Shekhar, M.; Wang, J.; Lee, W.-S.; Williams, W. D.; Kim, S. M.; Stach, E. A.; Miller, J. T.; Delgass, W. N.; Ribeiro, F. H. *J. Am. Chem. Soc.* **2012**, *134*, 4700−4708.
(8) Valden, M.; Lai, X.; Goodman, D. W. *Science* **1998**, *281*, 1647−1650.
(9) Herzing, A. A.; Kiely, C. J.; Carley, A. F.; Landon, P.; Hutchings, G. J. *Science* **2008**, *321*, 1331−1335.
(10) Chen, M. S.; Goodman, D. W. *Science* **2004**, *306*, 252−255.
(11) Falsig, H.; Hvolbæk, B.; Kristensen, I. S.; Jiang, T.; Bligaard, T.; Christensen, C. H.; Nørskov, J. K. *Angew. Chem., Int. Ed.* **2008**, *47*, 4835−4839.
(12) Lemire, C.; Meyer, R.; Shaikhutdinov, S.; Freund, H.-J. *Angew. Chem., Int. Ed.* **2004**, *43*, 118−121.
(13) Lopez, N.; Janssens, T. V. W.; Clausen, B. S.; Xu, Y.; Mavrikakis, M.; Bligaard, T.; Norskov, J. K. *J. Catal.* **2004**, *223*, 232−235.
(14) Mills, G.; Gordon, M. S.; Metiu, H. *J. Chem. Phys.* **2003**, *118*, 4198−4205.
(15) Saavedra, J.; Doan, H.; Pursell, C. J.; Grabow, L. C.; Chandler, B. D. *Science* **2014**, DOI: 10.1126/science.1256018.
(16) Oxford, S. M.; Henao, J. D.; Yang, J. H.; Kung, M. C.; Kung, H. H. *Appl. Catal., A* **2008**, *339*, 180−186.
(17) Menegazzo, F.; Manzoli, M.; Chiorino, A.; Boccuzzi, F.; Tabakova, T.; Signoretto, M.; Pinna, F.; Pernicone, N. *J. Catal.* **2006**, *237*, 431−434.
(18) Menegazzo, F.; Pinna, F.; Signoretto, M.; Trevisan, V.; Boccuzzi, F.; Chiorino, A.; Manzoli, M. *Applied Catalysis A: General* **2009**, *356*, 31−35.
(19) van Vegten, N.; Haider, P.; Maciejewski, M.; Krumeich, F.; Baiker, A. *J. Colloid Interface Sci.* **2009**, *339*, 310−316.
(20) Borgna, A.; Sepulveda, J.; Magni, S. I.; Apesteguia, C. R. *Appl. Catal., A* **2004**, *276*, 207−215.
(21) Park, S. H.; Rhee, H. K. *Appl. Catal., A* **2001**, *219*, 99−105.

DOI: 10.1021/cs501942t
ACS Catal. 2015, 5, 2232−2241

(22) Coughlan, B.; Keane, M. A. *J. Catal.* **1992**, *138*, 164−178.
(23) Simon, M. W.; Efstathiou, A. M.; Bennett, C. O.; Suib, S. L. *J. Catal.* **1992**, *138*, 1−11.
(24) Gonzalez-Tejuca, L.; Aika, K.; Namba, S.; Turkevich, J. *J. Phys. Chem.* **1977**, *81*, 1399−1406.
(25) Hornstein, B. J.; Aiken, J. D., III; Finke, R. G. *Inorg. Chem.* **2002**, *41*, 1625−1638.
(26) Bayram, E.; Linehan, J. C.; Fulton, J. L.; Roberts, J. A. S.; Szymczak, N. K.; Smurthwaite, T. D.; Ozkar, S.; Balasubramanian, M.; Finke, R. G. *J. Am. Chem. Soc.* **2011**, *133*, 18889−18902.
(27) Dehm, N. A.; Zhang, X.; Buriak, J. M. *Inorg. Chem.* **2010**, *49*, 2706−2714.
(28) Chandler, B. D.; Kendell, S.; Doan, H.; Korkosz, R.; Grabow, L. C.; Pursell, C. J. *ACS Catal.* **2012**, *2*, 684−694.
(29) Nigra, M. M.; Arslan, I.; Katz, A. *J. Catal.* **2012**, *295*, 115−121.
(30) Haider, P.; Urakawa, A.; Schmidt, E.; Baiker, A. *J. Mol. Catal. A: Chem.* **2009**, *305*, 161−169.
(31) Kahsar, K. R.; Schwartz, D. K.; Medlin, J. W. *J. Am. Chem. Soc.* **2014**, *136*, 520−526.
(32) Lien, C.-H.; Medlin, J. W. *J. Phys. Chem. C* **2014**, *118*, 23783−23789.
(33) Pang, S. H.; Schoenbaum, C. A.; Schwartz, D. K.; Medlin, J. W. *Nat. Commun.* **2013**, *4*, 3448−3454.
(34) Pang, S. H.; Schoenbaum, C. A.; Schwartz, D. K.; Medlin, J. W. *ACS Catal.* **2014**, *4*, 3123−3131.
(35) Bain, C. D.; Troughton, E. B.; Tao, Y. T.; Evall, J.; Whitesides, G. M.; Nuzzo, R. G. *J. Am. Chem. Soc.* **1989**, *111*, 321−335.
(36) Love, J. C.; Estroff, L. A.; Kriebel, J. K.; Nuzzo, R. G.; Whitesides, G. M. *Chem. Rev.* **2005**, *105*, 1103−169.
(37) Brust, M.; Walker, M.; Bethell, D.; Schiffrin, D. J.; Whyman, R. *J. Chem. Soc. Chem. Commun.* **1994**, 801−802.
(38) Boisselier, E.; Astruc, D. *Chem. Soc. Rev.* **2009**, *38*, 1759−1782.
(39) Daniel, M.-C.; Astruc, D. *Chem. Rev.* **2004**, *104*, 293−346.
(40) Lang, H.; May, R. A.; Iversen, B. L.; Chandler, B. D. *J. Am. Chem. Soc.* **2003**, *125*, 14832−4836.
(41) Pursell, C. J.; Chandler, B. D.; Manzoli, M.; Boccuzzi, F. *J. Phys. Chem. C* **2012**, *116*, 11117−1125.
(42) Pursell, C. J.; Hartshorn, H.; Ward, T.; Chandler, B. D.; Boccuzzi, F. *J. Phys. Chem. C* **2011**, *115*, 23880−23892.
(43) Hartshorn, H.; Pursell, C. J.; Chandler, B. D. *J. Phys. Chem. C* **2009**, *113*, 10718−10725.
(44) Karpovich, D. S.; Blanchard, G. J. *Langmuir* **1994**, *10*, 3315−3322.
(45) Ravi, V.; Binz, J. M.; Rioux, R. M. *Nano Lett.* **2013**, *13*, 4442−4448.
(46) Ansar, S. M.; Haputhanthri, R.; Edmonds, B.; Liu, D.; Yu, L.; Sygula, A.; Zhang, D. *J. Phys. Chem. C* **2011**, *115*, 653−660.
(47) Zhu, M.; Qian, H.; Jin, R. *J. Am. Chem. Soc.* **2009**, *131*, 7220−7221.
(48) Zeng, C.; Qian, H.; Li, T.; Li, G.; Rosi, N. L.; Yoon, B.; Barnett, R. N.; Whetten, R. L.; Landman, U.; Jin, R. *Angew. Chem., Int. Ed.* **2012**, *51*, 13114−13118.
(49) Jadzinsky, P. D.; Calero, G.; Ackerson, C. J.; Bushnell, D. A.; Kornberg, R. D. *Science* **2007**, *318*, 430−433.
(50) Bos, W.; Kanters, R. P. F.; Van Halen, C. J.; Bosman, W. P.; Behm, H.; Smits, J. M. M.; Beurskens, P. T.; Bour, J. J.; Pignolet, L. H. *J. Organomet. Chem.* **1986**, *307*, 385−398.
(51) Love, J. C.; Estroff, L. A.; Kriebel, J. K.; Nuzzo, R. G.; Whitesides, G. M. *Chem. Rev.* **2005**, *105*, 1103−1169.
(52) Fertitta, E.; Voloshina, E.; Paulus, B. *J. Comput. Chem.* **2014**, *35*, 204−13.
(53) Nadler, R.; Sanchez-de-Armas, R.; Sanz, J. F. *Comput. Theor. Chem.* **2011**, *975*, 116−121.
(54) Ford, M. J.; Hoft, R. C.; Gale, J. D. *Mol. Simul.* **2006**, *32*, 1219−1225.
(55) Higai, S. i.; Nara, J.; Ohno, T. *J. Chem. Phys.* **2004**, *121*, 970−972.
(56) Kato, H. S.; Noh, J.; Hara, M.; Kawai, M. *J. Phys. Chem. B* **2002**, *106*, 9655−9658.
(57) Hinterwirth, H.; Kappel, S.; Waitz, T.; Prohaska, T.; Lindner, W.; Lämmerhofer, M. *ACS Nano* **2013**, *7*, 1129−136.
(58) Hostetler, M. J.; Stokes, J. J.; Murray, R. W. *Langmuir* **1996**, *12*, 3604−1612.
(59) Luedtke, W. D.; Landman, U. *J. Phys. Chem. B* **1998**, *102*, 6566−6572.
(60) Lanterna, A. E.; Coronado, E. A.; Granados, A. M. *J. Phys. Chem. C* **2012**, *116*, 6520−6529.
(61) Majumder, C.; Mizuseki, H.; Kawazoe, Y. *J. Chem. Phys.* **2003**, *118*, 9809−9813.
(62) Elzey, S.; Tsai, D.-H.; Rabb, S. A.; Yu, L. L.; Winchester, M. R.; Hackley, V. A. *Anal. Bioanal. Chem.* **2012**, *403*, 145−149.
(63) Parks, G. A. *Chem. Rev.* **1965**, *65*, 177−198.
(64) Matthiesen, J. E.; Jose, D.; Sorensen, C. M.; Klabunde, K. J. *J. Am. Chem. Soc.* **2012**, *134*, 9376−9379.
(65) Balasubramanian, R.; Guo, R.; Mills, A. J.; Murray, R. W. *J. Am. Chem. Soc.* **2005**, *127*, 8126−8132.
(66) Kluth, G. J.; Carraro, C.; Maboudian, R. *Phys. Rev. B: Condens. Matter Mater. Phys.* **1999**, *59*, R10449−R10452.
(67) Ratnayake, S.; Dias, I. H. K.; Lattman, E.; Griffiths, H. R. *J. Proteomics* **2013**, *92*, 160−170.
(68) Le Moan, N.; Tacnet, F.; Toledano, M. B. *Methods Mol. Biol. (Totowa, N.J., U.S.)* **2008**, *476*, 181−198.
(69) Nagy, P. *Antioxid. Redox Signal.* **2013**, *18*, 1623−1641.
(70) Bricker, J. C.; Laricchia, L. *Top. Catal.* **2012**, *55*, 1315−1323.
(71) Fenter, P.; Eberhardt, A.; Eisenberger, P. *Science* **1994**, *266*, 1216−1218.
(72) Abad, A.; Corma, A.; Garcia, H. *Chem.−Eur. J.* **2008**, *14*, 212−222.
(73) Clément, M.; Ménard, H.; Rowntree, P. A. *Langmuir* **2008**, *24*, 8045−8049.
(74) Hasan, M.; Bethell, D.; Brust, M. *J. Am. Chem. Soc.* **2002**, *124*, 1132−1133.
(75) Ansar, S. M.; Perera, G. S.; Jiang, D.; Holler, R. A.; Zhang, D. *J. Phys. Chem. C* **2013**, *117*, 8793−8798.
(76) Vericat, C.; Vela, M. E.; Benitez, G.; Carro, P.; Salvarezza, R. C. *Chem. Soc. Rev.* **2010**, *39*, 1805−1834.
(77) Kankate, L.; Turchanin, A.; Goelzhauser, A. *Langmuir* **2009**, *25*, 10435−38.
(78) Hornstein, B. J.; Aiken, J. D.; Finke, R. G. *Inorg. Chem.* **2002**, *41*, 1625−1638.
(79) Fristrup, P.; Johansen, L. B.; Christensen, C. H. *Catal. Lett.* **2008**, *120*, 184−190.
(80) Conte, M.; Miyamura, H.; Kobayashi, S.; Chechik, V. *J. Am. Chem. Soc.* **2009**, *131*, 7189−196.
(81) Bayram, E.; Finke, R. G. *ACS Catal.* **2012**, *2*, 1967−1975.
(82) Merte, L. R.; Peng, G.; Bechstein, R.; Rieboldt, F.; Farberow, C. A.; Grabow, L. C.; Kudernatsch, W.; Wendt, S.; Laegsgaard, E.; Mavrikakis, M.; Besenbacher, F. *Science* **2012**, *336*, 889−893.

DOI: 10.1021/cs501942t
ACS Catal. 2015, 5, 2232−2241